AGU PUBLICATIONS

Geophysical Research Letters

RESEARCH LETTER
10.1002/2013GL058801

Key Points:
- Evanescent wave coupling links the solid Earth, oceans, and atmosphere
- Acoustic waves use anomalous transparency of the water-air interface
- Underwater geophysical processes and events can be heard in the atmosphere

Correspondence to:
L. G. Evers,
evers@knmi.nl

Citation:
Evers, L. G., D. Brown, K. D. Heaney, J. D. Assink, P. S. M. Smets, and M. Snellen (2014), Evanescent wave coupling in a geophysical system: Airborne acoustic signals from the M_w 8.1 Macquarie Ridge earthquake, *Geophys. Res. Lett.*, *41*, doi:10.1002/2013GL058801.

Received 25 NOV 2013
Accepted 8 JAN 2014
Accepted article online 14 JAN 2014

Evanescent wave coupling in a geophysical system: Airborne acoustic signals from the M_w 8.1 Macquarie Ridge earthquake

L. G. Evers[1,2], D. Brown[3], K. D. Heaney[4], J. D. Assink[5], P. S. M. Smets[1,2], and M. Snellen[6]

[1]Seismology Division, Royal Netherlands Meteorological Institute, De Bilt, Netherlands, [2]Department of Geoscience and Engineering, Faculty of Civil Engineering and Geosciences, Delft University of Technology, Delft, Netherlands, [3]International Data Center, Provisional Technical Secretariat, Comprehensive Nuclear-Test-Ban Treaty Organization, Vienna, Austria, [4]Ocean Acoustical Services and Instrumentation Systems, Inc., Lexington, Massachusetts, USA, [5]CEA, DAM, DIF, Arpajon, France, [6]Acoustic Remote Sensing Group, Faculty of Aerospace Engineering, Delft University of Technology, Delft, Netherlands

Abstract Atmospheric low-frequency sound, i.e., infrasound, from underwater events has not been considered thus far, due to the high impedance contrast of the water-air interface making it almost fully reflective. Here we report for the first time on atmospheric infrasound from a large underwater earthquake (M_w 8.1) near the Macquarie Ridge, which was recorded at 1325 km from the epicenter. Seismic waves coupled to hydroacoustic waves at the ocean floor, after which the energy entered the Sound Fixing and Ranging channel and was detected on a hydrophone array. The energy was diffracted by a seamount and an oceanic ridge, which acted as a secondary source, into the water column followed by coupling into the atmosphere. The latter results from evanescent wave coupling and the attendant anomalous transparency of the sea surface for very low frequency acoustic waves.

1. Introduction

The Comprehensive Nuclear-Test-Ban Treaty (CTBT) bans nuclear explosions by everyone, everywhere: on the Earth's surface, in the atmosphere, underwater, and underground. The International Monitoring System (IMS) consists of seismometers, hydrophones, and microbarometers to verify the treaty by measuring seismic waves in the solid Earth, hydroacoustic waves in the oceans, and infrasonic waves in the atmosphere. In addition, radionuclides and noble gases are measured in the atmosphere as a direct proof of a nuclear test explosion [*Dahlman et al.*, 2009].

One of the main sources of low-frequency waves detected by the IMS and other such networks are earthquakes, especially on the seismic and hydroacoustic components of the system [*De Groot-Hedlin*, 2005; *Guilbert et al.*, 2005]. Earthquakes on land are also a source of infrasonic signals in the atmosphere, but such signals are less often detected and are usually associated with large earthquakes [*Le Pichon et al.*, 2003; *Mutschlecner and Whitaker*, 2005].

A very large earthquake occurred near the Macquarie Ridge, southwest of New Zealand, on 23 December 2004 at 14h, 59min UTC. This earthquake received little attention, because of its isolated location and since it was followed about 58 h later by the devastating Sumatra earthquake and tsunami. The Global centroid moment tensor (CMT) Project located the earthquake at 161.35°E, 49.31°S [*Ekström et al.*, 2012], west of the Macquarie Ridge, which was later refined to 161.13°E, 49.96°S [*Robinson*, 2011]. With a magnitude M_w of 8.1, this event is one of the largest strike-slip events ever. Seismic signals were globally detected and will not be discussed [*Robinson*, 2011]. Here we will concentrate on the remarkable signals recorded on an eight element microbarometer array (IS05AU) operated by the CTBT Organization (CTBTO) as part of the IMS and on HA01W, a hydroacoustic triplet array (see Figure 1). These observations are explained by evanescent wave coupling which is known in acoustics, electromagnetics, and optics [*Pain*, 1983] but has not been reported in a geophysical system as resulting from an underwater earthquake. Evanescent wave coupling occurs when a sound source is located in water at a depth smaller compared to the acoustic wavelength, which makes the water-air interface anomalously transparent. There is a strong increase in the acoustic power flux in air; essentially, all low-frequency acoustic energy from the underwater source is radiated into the air.

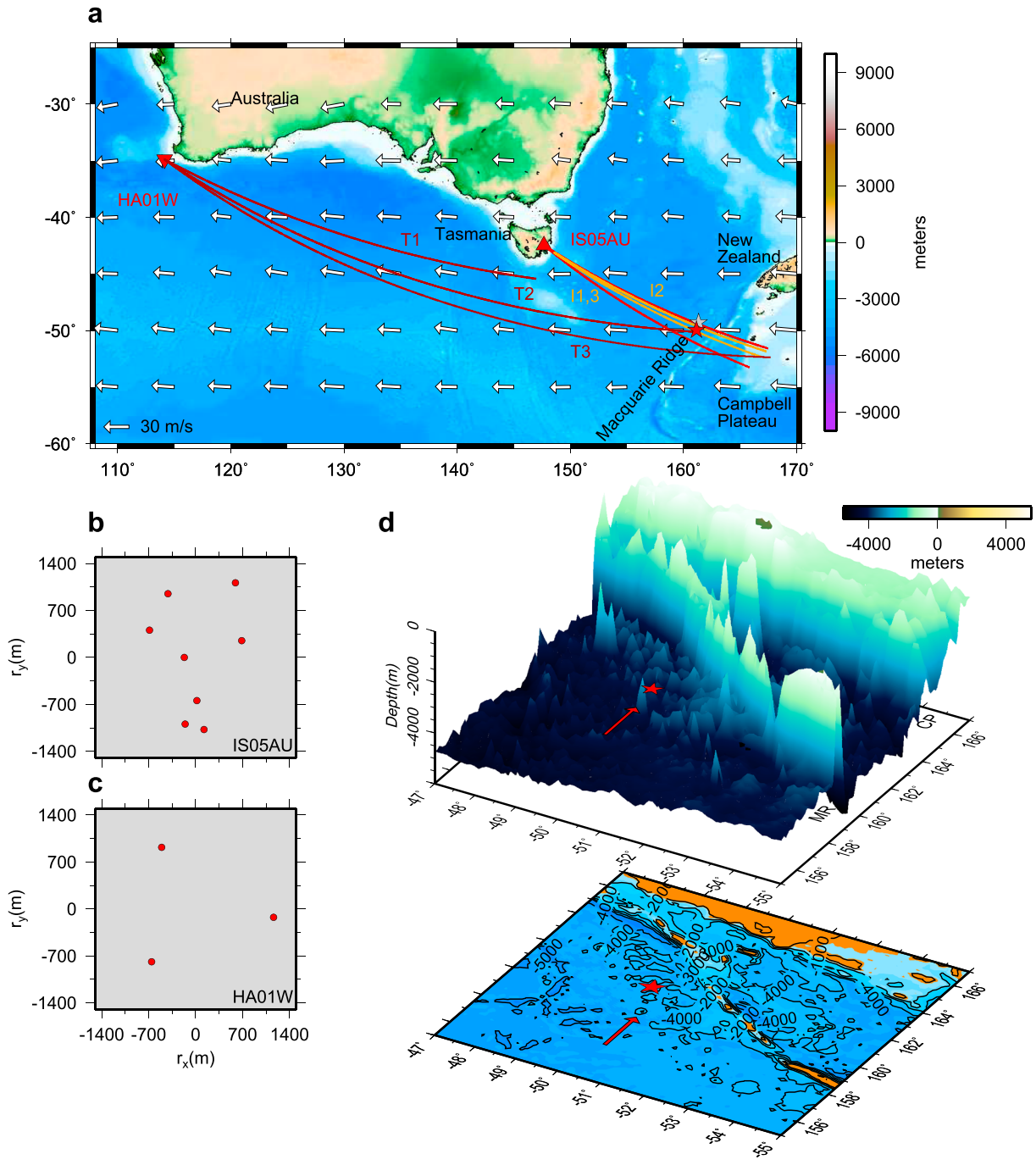

Figure 1. Map showing the location of the 23 December 2004 earthquake, the recording stations with the array layouts, and the bathymetry. (a) The location of the earthquake, near the Macquarie Ridge, is denoted by the stars. The gray star is the CMT solution, and the red star is the refined location. The color scheme gives the topography and bathymetry in meters; the water depth near the source is 4170 m. The triangle represents the location of the IMS infrasound array IS05AU in Tasmania (Australia). The inverted triangle gives the location of hydroacoustic array HA01W off the coast of southwestern Australia. The white arrows represent the wind strength and direction at an altitude of 40 km (3.36 hPa). The dark red lines are the back azimuths observed by HA01W. The red lines give the upper and lower limit of the observed back azimuth range by IS05AU; the orange lines are valid for the three infrasonic phases (I1, I3, and I2). (b) IS05AU is a 2.1 km aperture array consisting of eight microbarometers and is situated at a distance of 1325 km from the source. (c) HA01W is configured with three hydrophones with an aperture of 1.8 km and located 4129 km from the source. (d) The bathymetry showing the Macquarie Ridge (MR), Campbell Plateau (CP), and the earthquake location (red star). The red arrow points to a seamount nearby the epicenter, with its top at a depth of 2478 m following the ETOPO1 bathymetry [*Amante and Eakins*, 2009] and 1393 m from a local multibeam bathymetric survey (http://www.ga.gov.au/meta/ANZCW0703015735.html). Orange colors indicate potential secondary sources for an observed low-frequency cutoff of 1.3 Hz and 1485 m/s as propagation velocity.

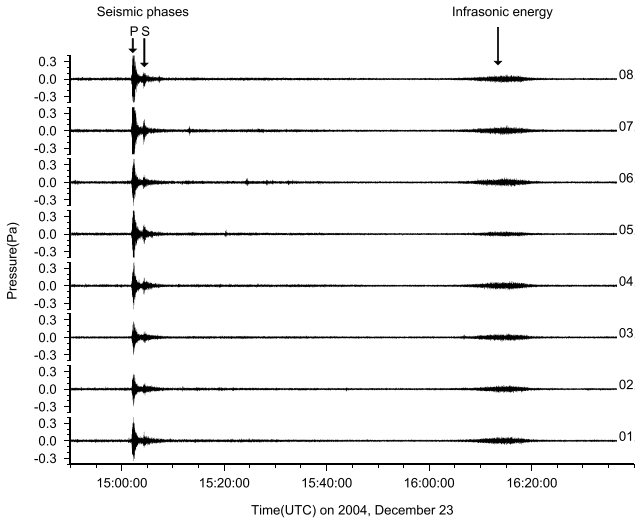

Figure 2. Recordings of the IMS infrasound array IS05AU on 23 December 2004 of the Macquarie Ridge earthquake. The atmospheric pressure fluctuations are shown as a function of time, from 14:50:00.00 to 16:40:00.00, and band pass filtered with a second order Butterworth filter with corner frequencies of 1.0 and 5.0 Hz. Each of the eight microbarometers of IS05AU measures at least three coherent arrivals. The first two arrivals are the seismic P and S phases that shook the microbarometers, which induced a pressure signal, and appeared between 15:01 and 15:05. Around 16:06 an atmospheric acoustic wave, i.e., infrasonic energy, unexpectedly arrives and lasts for about 16 min. The anomalous nature of this infrasonic wave is the subject of investigation in this study.

2. Infrasonic Observations

The signals as recorded by the infrasonic array IS05AU are shown in Figure 2. The first energy to arrive has a seismic origin and results from the movement of the bellows inside the microbarometer. In other words, the impulsive seismic P and S phases shake the instruments, which are located in a vault just beneath the Earth's surface, and leave their signature in the recordings. The first energy arrives 167 s after the earthquake occurred, which confirms the seismic cause, i.e., a propagation velocity of 7.9 km/s over 1325 km.

A second coherent package of energy arrives around 16h, 06min and lasts for 16 min. These signals are far more emergent than the seismic response and arrive with an average atmospheric velocity of 280 m/s, at maximum amplitude, which is calculated from the horizontal distance divided by traveltime and is called celerity. Such a celerity indicates that the energy has traveled through the stratosphere, where a downwind component is present (see Figure 1). The onset corresponds to a celerity of 330 m/s, which implies tropospheric propagation from the epicentral region.

Array processing techniques are applied to better associate the infrasonic signals to the epicentral region [*Evers and Haak*, 2001]. Figure 2 shows the results of such an analysis. The signal coherency increases around the time of arrival of the transients, while an average apparent velocity of 340 m/s, i.e., the propagation velocity over the array, is resolved. This velocity corresponds to the local sound speed. The energy comes from a southeasterly direction, and the observed back azimuth fluctuates around the epicenter's back azimuth. This all indicates that the infrasonic energy came from the epicentral area. Propagation modeling with atmospheric specification from the European Centre of Medium-Range Weather Forecasts (ECMWF) confirms the existence of a stratospheric duct between the source and receiver (Figure 4). The modeling predicts an average celerity of 282 m/s. Three infrasound phases (I1, I2, and I3) are identified in the recordings.

The correspondence between observations and modeling makes it highly likely that the infrasound is caused by the earthquake. But what can be the cause of this atmospheric infrasound from a source buried under 4170 m of water?

3. Hydroacoustical Observations

The acoustic transparency of the water-air interface is defined as the ratio of the acoustic power radiated into air to the total power radiated by an underwater continuous wave source. With the large mass density

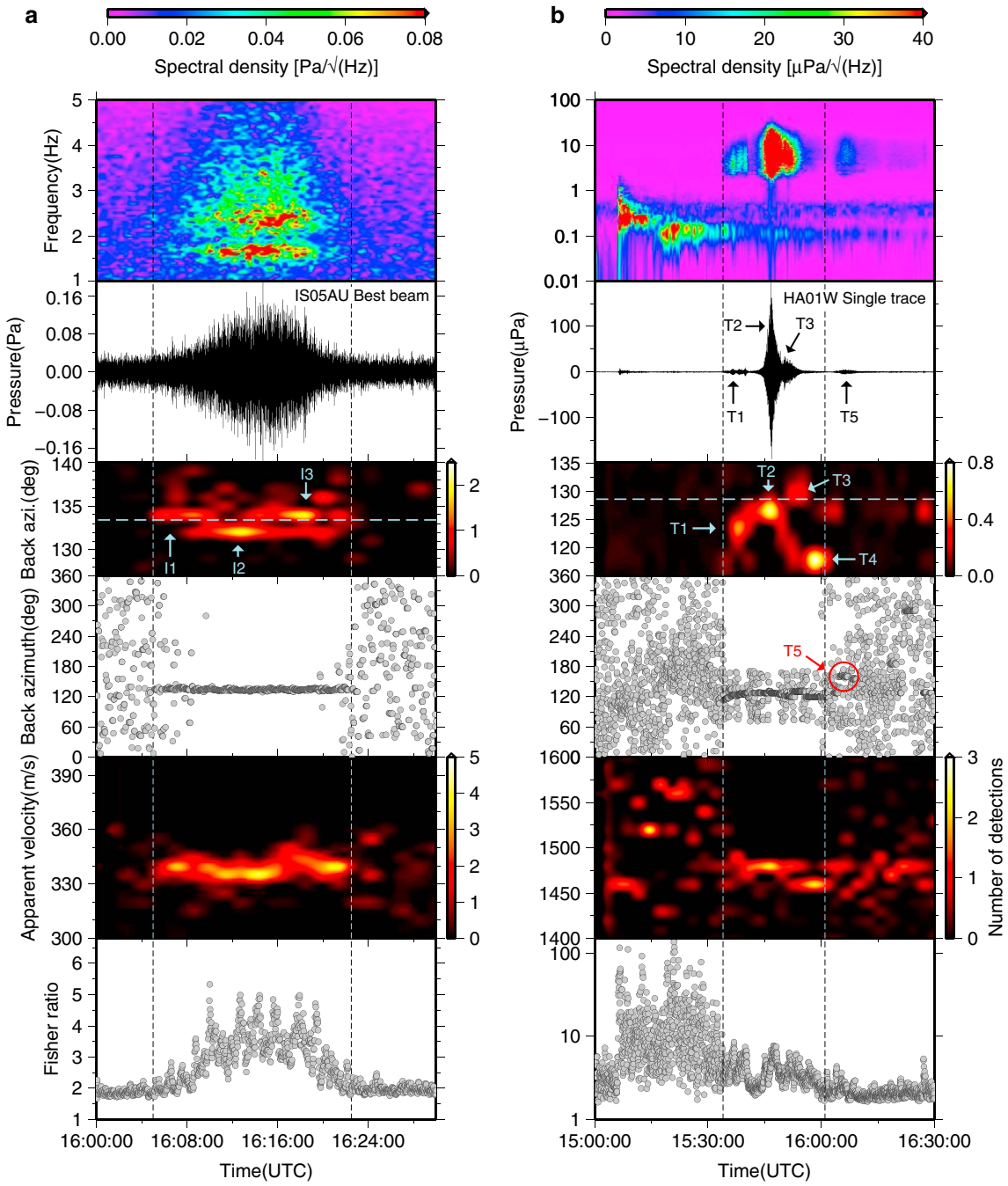

Figure 3. Array processing results of infrasound array IS05AU and hydroacoustic array HA01W. (a) The results of a Fisher ratio detector and beamforming for IS05AU. From bottom to top are given as a function of time: the Fisher ratio, i.e., a measure of the signal-to-noise ratio [*Evers and Haak*, 2001], apparent velocity (number of detections averaged per 2 min and 5 m/s), back azimuth, and zoom in (averaged per 2 min and 1°) around the epicenter's back azimuth (dashed line at 133.4°), best beam, and its spectrogram. The data are prefiltered with a second order Butterworth filter with corner frequencies of 1.0 to 5.0 Hz and split in time windows of 12.8 s. For each window, the Fisher ratio is calculated with 12.5% overlap. The maximum Fisher ratio per window is shown and its corresponding apparent velocity and back azimuth from beamforming. A total of 40,000 beams are generated on a slowness grid from −0.005 to 0.005 s/m. The best beam is the sum of the time-aligned traces for the slowness corresponding to the maximum Fisher ratio over the whole time period (around 16:10). The spectrogram is calculated with a fast Fourier transform with a sliding window size of 25.6 s and 50% overlap. (b) The processing results for HA01W. The processing parameters are the following: filter from 0.01 to 20 Hz, a total of 10,000 beams between −0.001 and 0.001 s/m, and a time window of 4.1 s with 50% overlap. The apparent velocity values are averaged over 3 min and 10 m/s. The back azimuth zoom in is averaged for 3 min and 3°. The trace shown is the recording from hydrophone W1 of HA01W, and its spectrogram is calculated with a window size of 32. 8 s with 50% overlap. Since the energy comes from different directions, no best beam can be formed. The label T2 points to the main T phase, which is preceded by T1, and T3, T4, and T5 are additional T phases.

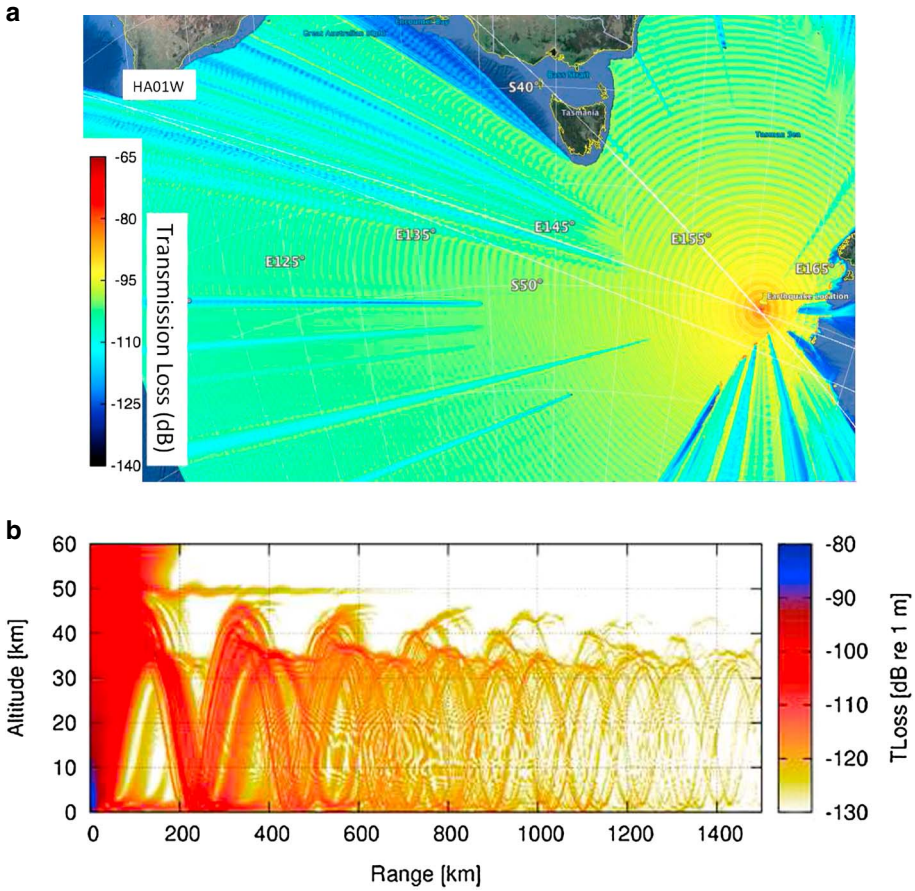

Figure 4. Hydroacoustic propagation from the source to HA01W and infrasonic propagation toward IS05AU. (a) Hydroacoustic propagation as modeled with a 3-D parabolic equation method at 5 Hz [*Collins*, 1993]. T phases are generated at the source and propagate through the SOFAR channel, with its axis around 1200 m water depth. There is a direct path from the source to the receiver, which results in T2 (see Figure 2). Phase T3 results from the reflection of the Campbell Plateau (see also Figure 1), and T4 is a reflection of the southern tip of Tasmania. The Macquarie Ridge clearly interrupts the hydroacoustic propagation as it cuts through the SOFAR channel. (b) The propagation of the infrasound through the atmosphere is modeled with the parabolic equation and valid for a signal of 1.6 Hz, which is the dominant frequency of the observed signals at IS05AU [*Collins*, 1993]. The atmospheric specifications are from the ECMWF and representative for 23 December 2004 at 18 UTC. Such specifications are available on a 0.5 by 0.5° spatial grid. Range-dependent wind and temperature specifications are derived between the source and receiver and form the input for the parabolic equation calculations. Shown is the transmission loss as a function of altitude and distance; the energy is refracted around the stratopause. Energy is emitted by the source directly into the stratosphere, and some are leaking into the stratosphere through the tropopause.

(factor of 800) and velocity contrast, the water-air interface is normally considered to have an acoustic transparency of a few hundredths of a percent and to be almost perfectly reflecting [*Leighton*, 2012].

The sea surface itself can generate infrasound, when interfering oceanic waves near depressions and storms lead to standing waves that emit acoustic waves into the ocean and atmosphere [*Waxler and Gilbert*, 2006]. Such waves are globally detected on seismometers as microseisms and as microbaroms on microbarometers and are often labeled as noise [*Donn and Rind*, 1971; *Evers and Haak*, 2001]. However, in the present case the acoustic energy must have coupled from the seismic energy, on the ocean floor, into the ocean, and then through the water-air interface into the atmosphere. Evanescent wave coupling between the ocean and the atmosphere has theoretically been shown for very low frequency waves. The water-air interface becomes anomalously transparent if the wavelength of the acoustic wave in water is significantly larger than the source depth [*Godin*, 2006, 2008a, 2008b].

In order to get insight into the energy that was radiated into the ocean, the recordings at hydroacoustic array HA01W are analyzed. Figure 2b shows the results of the hydroacoustic array processing. The first

energy to arrive is the P phase that hit the ocean floor beneath the array, shaking the hydrophones that are mounted to the seabed. After about 15 min, a dispersive and a lower frequency wave arrives, i.e., the seismic Rayleigh surface wave. The continuous band of energy around 0.2 Hz is caused by the nonlinear interaction of oceanic waves, as discussed above. Between 15:35 and 16:00, acoustic energy is detected with velocities around 1475 m/s from the correct back azimuth.

The hydroacoustic waves are so-called T phases and propagated through the SOFAR channel, with its axis at a water depth of 1200 m [*Okal*, 2001]. The limited thickness of the SOFAR channel of about 1 km is echoed in the frequency contents of the recording of one of the array elements, which shows a low-frequency cutoff of about 1.5 Hz. The back azimuths seem to be bounded to a range of 60 to 180°, which is likely controlled by reflections off the southern coast of Australia and Antarctica. The main T phase (labeled as T2 in Figure 2), associated to the rupture, arrives with a back azimuth close to the true back azimuth; after 5 min a second T phase (T3) arrives with a more southerly back azimuth of 131°, followed by T4 and T5. Phase T2 is preceded by a low-amplitude T phase, which is labeled as T1.

4. Evanescent Wave Coupling

The infrasound generating mechanism can be understood as follows. The *P* wave and vertically polarized *S* wave impinged on the ocean floor and generated an acoustic wave in the ocean. The energy coupled into the SOFAR channel and started propagating as a T phase in all directions. A nearby seamount and the Macquarie Ridge cut through the SOFAR channel and were hit by the T phase (see Figure 1). The seamount and the ridge acted as secondary sources (Huygens' principle) and diffracted acoustic energy into the SOFAR channel and (upward) into the water column. The frequency contents of the radiated acoustic waves by the secondary source is also about 1.5 Hz and higher. Near the seamount (with its top at a depth of 1393 m) and the ridge, the hydroacoustic wavelength is close to or more than the source depth. As a result, the water-air interface becomes anomalously transparent and hydroacoustic energy couples to atmospheric infrasound. The infrasound then propagates to IS05AU, where it appears with the same low-frequency contents as the T phase.

Propagation modeling with a 3-D parabolic equation code and a point source showed that T2 was generated near the epicenter and that T3 follows from reflections off the edge of the Campbell Plateau (see Figure 4). T4 is a reflection of the southern tip of Tasmania, and T5 is a reflection of Antarctica. The precursory T phase T1 finds its origin at the Tasmania Island Ridge, where the seismic *P* wave induced a hydroacoustic signal. Both the observed and modeled back azimuths and traveltimes are in agreement. With a similar technique, the 2-D atmospheric propagation was modeled for a point source [*Collins*, 1993]. The arrival time of the first energy (I1) requires passage through the troposphere and results from the diffraction of acoustic waves by a shallow seamount near the epicenter (see Figure 1), with its top in the SOFAR channel.

The energy related to I2 and I3 was generated at the Macquarie Ridge, cutting through the SOFAR channel and acting as a secondary source. Although the modeling only predicts stratospheric phases in the far field (see Figure 4), uncertainties in the atmospheric models and fine-scale atmospheric structure will allow for the existence of a (weak) tropospheric duct, as present near the source region. The observed back azimuth range is consistent with the proposed source locations; crosswinds along the source-receiver trajectory result in azimuthal deviations of several degrees.

As described by *Godin* [2008b], long-range infrasound propagation through the atmospheric waveguides is facilitated by the sea surface roughness and the generation of normal modes. Both these factors allow for the infrasound to enter the waveguides at suitable angles, where in a ray theoretical approach most energy would be radiated vertically (up to 13° of vertical) and be lost in the thermosphere.

It should also be noted that the transparency near the seamount is disputable, because the depth of the acoustic source (1325 m) is close to a wavelength near the seamount. This wavelength is 1142 m which follows from a propagation velocity of 1485 m/s and low-frequency cutoff of 1.3 Hz (see Figure 2). The frequency contents of the infrasound is slightly lower than the T phases, which might be caused by a thicker SOFAR channel in the deep sea versus the size near the coast at HA01W.

An alternative explanation for the infrasound observations could come from an island with topography (see, for example, *Walker et al.* [2013]), where seismic waves generate atmospheric infrasound. However, the

nearest island is the Macquarie Island, and both the observed back azimuth and traveltime do not support this source location.

5. Conclusions

In conclusion, we have shown for the first time observationally that the water-air interface can become anomalously transparent, if the hydroacoustic wavelength is significantly larger than the source depth, in a geophysical system due to an underwater earthquake. The observations support the theory that low-frequency underwater sources can acoustically be detected in the atmosphere from the evanescent wavefield [*Godin*, 2006, 2008a, 2008b], which has been shown on a small scale with laboratory experiments [*Calvo et al.*, 2013]. Applications are foreseen in land-based monitoring of underwater geophysical processes, like underwater volcanic eruptions [*Green et al.*, 2013] and earthquakes. Furthermore, the detection and localization of underwater explosions, as those monitored with, for example, the IMS, can be enhanced with the inclusion of the infrasonic component [*Prior et al.*, 2011]. The question of how underwater sources contribute to the ambient atmospheric noise field also arises, which in turn can be used for imaging of the (upper) atmosphere [*Haney*, 2009; *Fricke et al.*, 2013].

Acknowledgments

P.S.M. Smets and J.D. Assink appreciate the support of the ARISE collaborative project, funded by the European Union (http://arise-project.eu). The CTBTO and station operators are thanked for guaranteeing the high quality of the IMS data and products. M.K. Prior (CTBTO) is thanked for his input on technical and observational issues. Figures in this article were made with the Generic Mapping Tools [*Wessel and Smith*, 1991]. We thank D.N. Green and an anonymous reviewer for their reviews which helped in improving the manuscript.

The Editor thanks David Green and an anonymous reviewer for their assistance in evaluating this paper.

References

Amante, C., and B. W. Eakins, (2009), ETOPO1 1 arc-minute global relief model: Procedures, data sources and analysis, *Tech. Rep. NESDIS NGDC-24*, National Oceanic and Atmospheric Administration.

Calvo, D. C., M. Nicholas, and G. J. Orris (2013), Experimental verification of enhanced sound transmission from water to air at low frequencies, *J. Acoust. Soc. Am.*, *134*, 3403–3408.

Collins, M. D. (1993), A split-step Padé solution for the parabolic equation method, *J. Acoust. Soc. Am.*, *93*, 1736–1742.

Dahlman, O., S. Mykkeltveit, and H. Haak (2009), *Nuclear Test Ban*, 113–142 pp., Springer, Dordrecht, Netherlands.

De Groot-Hedlin, C. D. (2005), Estimation of the rupture length and velocity of the Great Sumatra earthquake of Dec 26, 2004 using hydroacoustic signals, *Geophys. Res. Lett.*, *32*, L11303, doi:10.1029/2005GL022695.

Donn, W. L., and D. Rind (1971), Natural infrasound as an atmospheric probe, *Geophys. J. R. Astron. Soc.*, *26*, 111–133.

Ekström, G., M. Nettles, and A. M. Dziewoński (2012), The global CMT project 2004–2010: Centroid-moment tensors for 13,017 earthquakes, *Phys. Earth Planet. Inter.*, *200-201*, 1–9.

Evers, L. G., and H. W. Haak (2001), Listening to sounds from an exploding meteor and oceanic waves, *Geophys. Res. Lett.*, *28*, 41–44.

Fricke, J. T., N. El Allouche, D. G. Simons, E. N. Ruigrok, K. Wapenaar, and L. G. Evers (2013), Infrasonic interferometry of stratospherically refracted microbaroms—A numerical study, *J. Acoust. Soc. Am.*, *134*, 2660–2668.

Godin, O. A. (2006), Anomalous transparency of water-air interface for low-frequency sound, *Phys. Rev. Lett.*, *97*, 164301.

Godin, O. A. (2008a), Low-frequency sound transmission through a gas-liquid interface, *J. Acoust. Soc. Am.*, *123*, 1866–1879.

Godin, O. A. (2008b), Sound transmission through water–air interfaces: New insights into an old problem, *Contemp. Phys.*, *49*, 105–123.

Green, D. N., L. G. Evers, D. Fee, R. S. Matoza, M. Snellen, P. Smets, and D. Simons (2013), Hydroacoustic, infrasonic and seismic monitoring of the submarine eruptive activity and sub-aerial plume generation at South Sarigan, May 2010, *J. Volcanol. Geotherm. Res.*, *257*, 31–43.

Guilbert, J., J. Vergoz, E. Schisselé, A. Roueff, and Y. Cansi (2005), Use of hydroacoustic and seismic arrays to observe rupture propagation and source extent of the Mw = 9.0 Sumatra earthquake, *Geophys. Res. Lett.*, *32*, L15310, doi:10.1029/2005GL022966.

Haney, M. M. (2009), Infrasonic ambient noise interferometry from correlations of microbaroms, *Geophys. Res. Lett.*, *36*, L19808, doi:10.1029/2009GL040179.

Le Pichon, A., J. Guilbert, M. Valleé, J. X. Dessa, and M. Ulziibat (2003), Infrasonic imaging of the Kunlun Mountains for the great 2001 China earthquake, *Geophys. Res. Lett.*, *30*(15), 1814, doi:10.1029/2003GL017581.

Leighton, T. G. (2012), How can humans, in air, hear sound generated underwater (and can goldfish hear their owners talking)?, *J. Acoust. Soc Am.*, *131*, 2539–2542.

Mutschlecner, J. P., and R. W. Whitaker (2005), Infrasound from earthquakes, *J. Geophys. Res.*, *110*, D01108, doi:10.1029/2004JD005067.

Okal, E. A. (2001), T-phase stations for the International Monitoring System of the Comprehensive Nuclear-Test Ban Treaty: A global perspective, *Seismol. Res. Lett.*, *72*, 186–196.

Pain, H. J. (1983), *The Physics of Vibration and Waves*, 237–240 pp., Wiley, Chichester, U. K.

Prior, M. K., O. Meless, P. Bittner, and H. Sugioka (2011), Long-range detection and location of shallow underwater explosions using deep-sound-channel hydrophones, *IEEE J. Oceanic Eng.*, *36*, 703–715.

Robinson, D. P. (2011), A rare great earthquake on an oceanic fossil fracture zone, *Geophys. J. Int.*, *186*, 1121–1134.

Walker, K. T., A. Le Pichon, T. S. Kim, C. de Groot-Hedlin, I.-Y. Che, and M. Garcés (2013), An analysis of ground shaking and transmission loss from infrasound generated by the 2011 Tohoku earthquake, *J. Geophys. Res. Atmos.*, *118*, 12,805-12,815, doi:10.1002/2013JD020187.

Waxler, R., and K. E. Gilbert (2006), The radiation of atmospheric microbaroms by ocean waves, *J. Acoust. Soc. Am.*, *119*, 2651–2664.

Wessel, P., and W. H. F. Smith (1991), Free software helps map and display data, *EOS Trans. AGU*, *72*, 441–446.